# Effect of Carbon Concentration on Precipitation Behavior of $M_{23}C_6$ Carbides and MX Carbonitrides in Martensitic 9Cr Steel during Heat Treatment

MASAKI TANEIKE, KOTA SAWADA, and FUJIO ABE

The distributions and precipitated amounts of $M_{23}C_6$ carbides and MX-type carbonitrides with decreasing carbon content from 0.16 to 0.002 mass pct in 9Cr-3W steel, which is used as a heat-resistant steel, has been investigated. The microstructures of the steels are observed to be martensite. Distributions of precipitates differ greatly among the steels depending on carbon concentration. In the steels containing carbon at levels above 0.05 pct, $M_{23}C_6$ carbides precipitate along boundaries and fine MX carbonitrides precipitate mainly in the matrix after tempering. In 0.002 pct C steel, there are no $M_{23}C_6$ carbide precipitates, and instead, fine MX with sizes of 2 to 20 nm precipitate densely along boundaries. In 0.02 pct C steel, a small amount of $M_{23}C_6$ carbides precipitate, but the sizes are quite large and the main precipitates along boundaries are MX, as with 0.002 pct C steel. A combination of the removal of any carbide whose size is much larger than that of MX-type nitrides, and the fine distributions of MX-type nitrides along boundaries, is significantly effective for the stabilization of a variety of boundaries in the martensitic 9Cr steel.

## I. INTRODUCTION

FERRITIC heat-resistant steels have attracted strong interest in applications for boilers and turbines of ultra super critical power plants. These steels require a long duration of service, often greater than 10 years. Creep strength is the most important property for these steels, but the creep strength usually decreases during long-term use because the microstructure of the steel changes gradually at high temperatures. Consequently, there is a strong demand for further improvement of long-term creep strength and prevention of the decrease in creep strength caused by changes of the steel microstructure. In particular, the agglomeration and coarsening of precipitates have the largest influence on the reduction of long-term creep strength.[1]

In 9-12Cr steels, various precipitate particles can be observed. $M_{23}C_6$ carbides and MX-type carbonitrides are mentioned as primary examples. $M_{23}C_6$ carbides mainly precipitate along prior austenite grain boundaries and boundaries with a large angle, such as block and packet boundaries of martensite. It is assumed that they are effective in strengthening boundaries, since $M_{23}C_6$ carbides act as obstacles for migrating boundaries. However, they tend to coarsen easily during creep because solubility of iron and chromium, which are major constituents of $M_{23}C_6$, is large. Accordingly, prevention of coarsening of $M_{23}C_6$ carbides is important for improving creep strength. Abe[2] reported that coarsening of $M_{23}C_6$ carbides containing tungsten occurs more slowly since tungsten has low diffusion coefficients, and hence creep life extends. From a different point of view, Horiuchi *et al.*[3] has suggested that adding boron in $M_{23}C_6$ carbides stabilizes the microstructure near prior austenite grain boundaries, which increases long-term creep strength.

The MX carbonitrides precipitate mainly along dislocations in the matrix of martensitic lath. The size of MX is very small (about 2 to 20 nm), while the size of $M_{23}C_6$ is about 200 to 300 nm.[4] It is considered that MX particles work as obstructions to moving of dislocations in the matrix. Since MX carbonitrides are mainly composed of niobium and vanadium whose solubility is quite small in the ferrite matrix, they do not grow easily during high-temperature creep.

Up to now, it has been considered that $M_{23}C_6$ carbides strengthen boundaries, and MX carbonitrides strengthen the matrix by acting as obstructions to the moving of dislocations, since $M_{23}C_6$ carbides precipitate along boundaries and MX precipitate mainly in the matrix. For precipitation strengthening, MX carbonitrides are more advantageous than $M_{23}C_6$ carbides because MX precipitate finely and densely and do not grow easily at high temperatures. The effect of precipitation strengthening is in inverse proportion to the spacing between particles.[5] If fine MX can be made to distribute densely also along boundaries in place of large $M_{23}C_6$ carbides, it should be possible to improve creep strength. In conventional 9-12 Cr steel, MX precipitates mainly in the matrix, but it is possible that MX can be made to precipitate along boundaries by getting rid of $M_{23}C_6$. Since $M_{23}C_6$ is carbide and MX is carbonitride, it is possible that $M_{23}C_6$ carbides are reduced and only MX nitrides precipitate by decreasing carbon content. The feasibility of applying only MX nitrides for improvement of creep strength has not been studied with regard to 9-12Cr steel, which normally uses $M_{23}C_6$ for strengthening.

The purpose of this study is to investigate precipitation behavior with decreasing carbon content from 0.16 to 0.002 mass pct in 9Cr-3W steel, which has drawn attention in the ultra steel project of NIMS.[6] In addition, the study verifies the fine distribution of the MX nitrides along prior austenite grain boundaries and block boundaries. The creep strength of the steel, which has a distribution of fine MX along boundaries, improves extremely.[7]

MASAKI TANEIKE and KOTA SAWADA, Researchers, and FUJIO ABE, Director, are with the Steel Research Center, National Institute for Materials Science, Tsukuba 305-0047, Japan. Contact e-mail: abe.fujio@nims.go.jp

Manuscript submitted May 30, 2003.

## II. ESTIMATION OF EFFECT OF CARBON CONTENT ON PRECIPITATES

In order to estimate the change of equilibrium amount of MX and $M_{23}C_6$ with decreasing carbon content at 1073 K, which is the conventional tempering temperature, calculation by Thermo-Calc[8] was carried out. The base composition used in the calculation was 9Cr-0.3Si-0.5Mn-3W-0.2V-0.06Nb-3Co-0.05N-0.007B-C. The equilibrium amount of precipitates and the fraction of constituents in MX calculated by Thermo-Calc are shown in Figures 1 and 2, respectively.

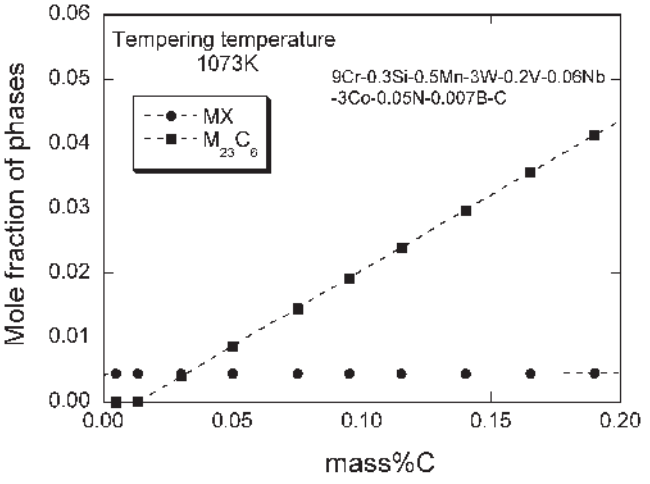


Fig. 1—Equilibrium mole fraction of phases at 1073 K calculated by Thermo-Calc.

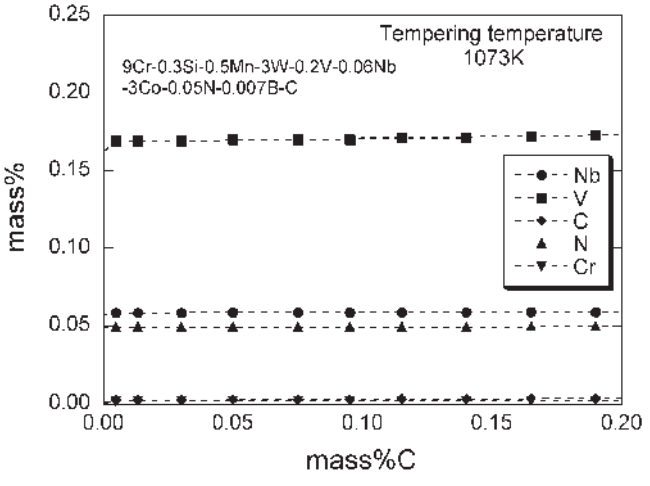


Fig. 2—Equilibrium precipitated amount of elements contained in MX at 1073 K calculated by Thermo-Calc.

The amount of $M_{23}C_6$ decreased with decreasing carbon content and the amount of MX was larger than that of $M_{23}C_6$ in the range of carbon content below 0.02 pct. As shown in Figure 2, MX are almost all nitrides in the calculation and hence the change of carbon content does not greatly influence the amount and the composition of MX. It is believed that decreasing carbon content causes MX nitrides to precipitate along boundaries instead of $M_{23}C_6$ carbides.

## III. EXPERIMENTAL PROCEDURE

The chemical compositions of the steels used in this study are given in Table I. They are based on 9Cr-3W-3Co-0.05N-0.007B, similarly to those of conventional 9Cr steel. The concentration of carbon varied widely from 0.002 to 0.160 mass pct. No carbon was added in the 0.002 pct C steel. These steels are designated 0C, 02C, 05C, 08C, 12C, and 16C, corresponding to the concentration of carbon. The steels were melted as 50-kg ingots in a vacuum induction furnace and forged into bars with diameters of 25 mm. They were normalized at 1373 K for 0.5 hours, cooled in air, and then tempered at 1073 K for 1 hour. The curves of thermal expansion of the steels were measured by a Formastor-F2 (Fuji Electronic Industrial Co. Ltd., Saitama, Japan), with cooling and heating rates of 20 °C/min. Transformation temperatures of the steels were determined from the local maximal values and local minimal values of the curves of the thermal expansion. Vickers hardness levels of the steels after tempering and after normalizing were measured under loading condition of 10 kg for 15 seconds. The microstructures of the steels were observed by using a 200 kV transmission electron microscope (TEM, JEOL* 2010F), using thin films and carbon extraction replicas. The compositions of the observed precipitates were analyzed by an energy-dispersive X-ray (EDX) analyzer attached to the TEM. Lath width and dislocation density were estimated by the line-crossing method[9] from photographs of thin foils by TEM. The concentration of alloying elements in precipitates was analyzed using the ICP method with residues extracted electrolytically.

*JEOL is a trademark of Japan Electron Optics Ltd., Tokyo.

## IV. RESULTS

### A. *Morphology of Martensitic Microstructure after Normalizing and Tempering*

Figure 3 shows transformation temperature, $Ac_1$, $M_s$, and $M_f$, in the steels. The $Ac_1$ temperatures are almost the same in all the steels. The $M_s$ and $M_f$ temperatures increase with

**Table I. Chemical Compositions of the Steels Studied (Mass Percent)**

| Steel | C | Si | Mn | Cr | W | V | Nb | Co | N | B |
|---|---|---|---|---|---|---|---|---|---|---|
| 0C | 0.002 | 0.29 | 0.51 | 9.19 | 2.96 | 0.20 | 0.060 | 3.09 | 0.049 | 0.0070 |
| 02C | 0.018 | 0.29 | 0.50 | 9.16 | 2.91 | 0.20 | 0.058 | 2.94 | 0.050 | 0.0068 |
| 05C | 0.047 | 0.30 | 0.51 | 9.24 | 2.90 | 0.20 | 0.059 | 3.07 | 0.050 | 0.0063 |
| 08C | 0.078 | 0.31 | 0.51 | 9.26 | 2.93 | 0.20 | 0.061 | 3.08 | 0.049 | 0.0064 |
| 12C | 0.120 | 0.30 | 0.50 | 9.27 | 2.93 | 0.20 | 0.058 | 3.08 | 0.048 | 0.0065 |
| 16C | 0.160 | 0.30 | 0.51 | 9.26 | 2.94 | 0.20 | 0.058 | 3.06 | 0.047 | 0.0061 |

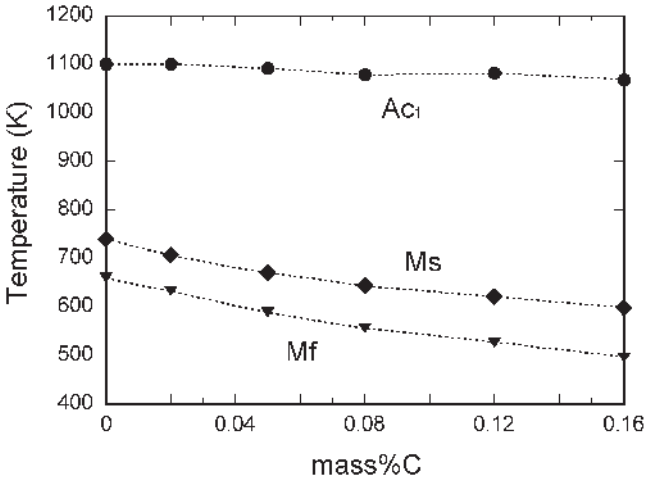


Fig. 3—Transformation temperature of the steels.

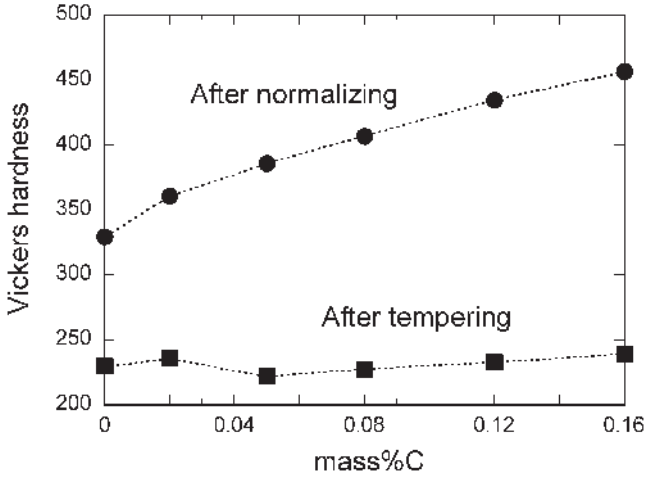


Fig. 4—Vickers hardness levels of the steels after normalizing and tempering.

decreasing carbon content. The temperatures of 0C steel are about 100 K higher than those of 16C steel.

Figure 4 shows the Vickers hardness levels of the steels after normalizing and after tempering. The hardness after tempering is similar in all the steels. In contrast, the hardness after normalizing decreases with decreasing carbon content. It is reported that $M_s$ and $M_f$ temperatures decrease, and hardness after normalizing increases with increasing carbon content, due to solid solution strengthening by supersaturated carbon in the steels.[10] The values of the Vickers hardness levels after tempering are similar in all the steels since supersaturated carbon precipitates as carbides.

In order to investigate in detail the differences in martensitic microstructure with the difference of carbon concentration, observation of the microstructure by the TEM was carried out. Figure 5 shows the TEM micrographs of thin films of 0C and 08C steels after normalizing. The microstructure of 0C steel, which contains almost no carbon, is also martensite, like 08C steel. Figure 6 shows the lath widths and dislocation densities in 0C and 08C steels after normalizing and tempering. The dislocation densities in the steels after normalizing are about $10^{15}$ $m^{-2}$ order and those

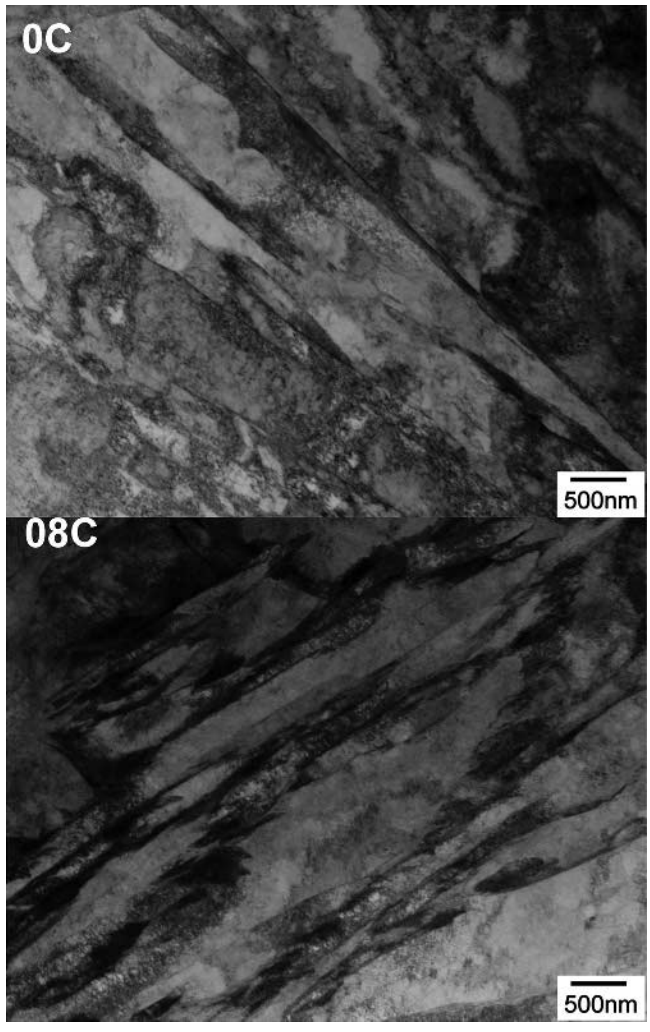


Fig. 5—TEM micrographs of thin films of 0C and 08C steel after normalizing.

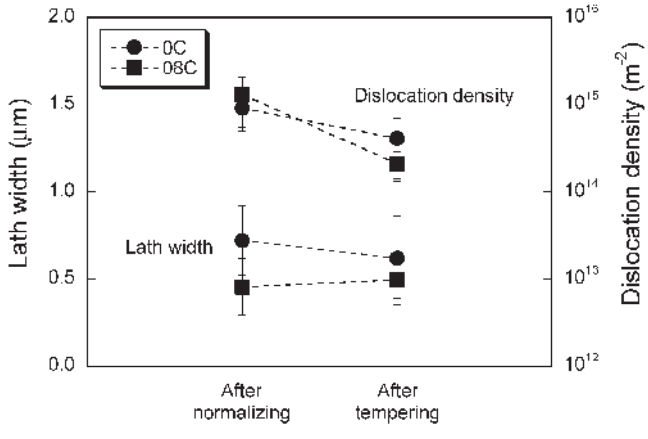


Fig. 6—Lath width and dislocation density of 0C and 08C steels after each heat treatment.

after tempering decrease to $10^{14}$ $m^{-2}$ order. The dislocation densities between 0C and 08C steels are not so different. The lath widths in 08C steel are smaller than those in 0C steel, but the difference is quite small. The difference of

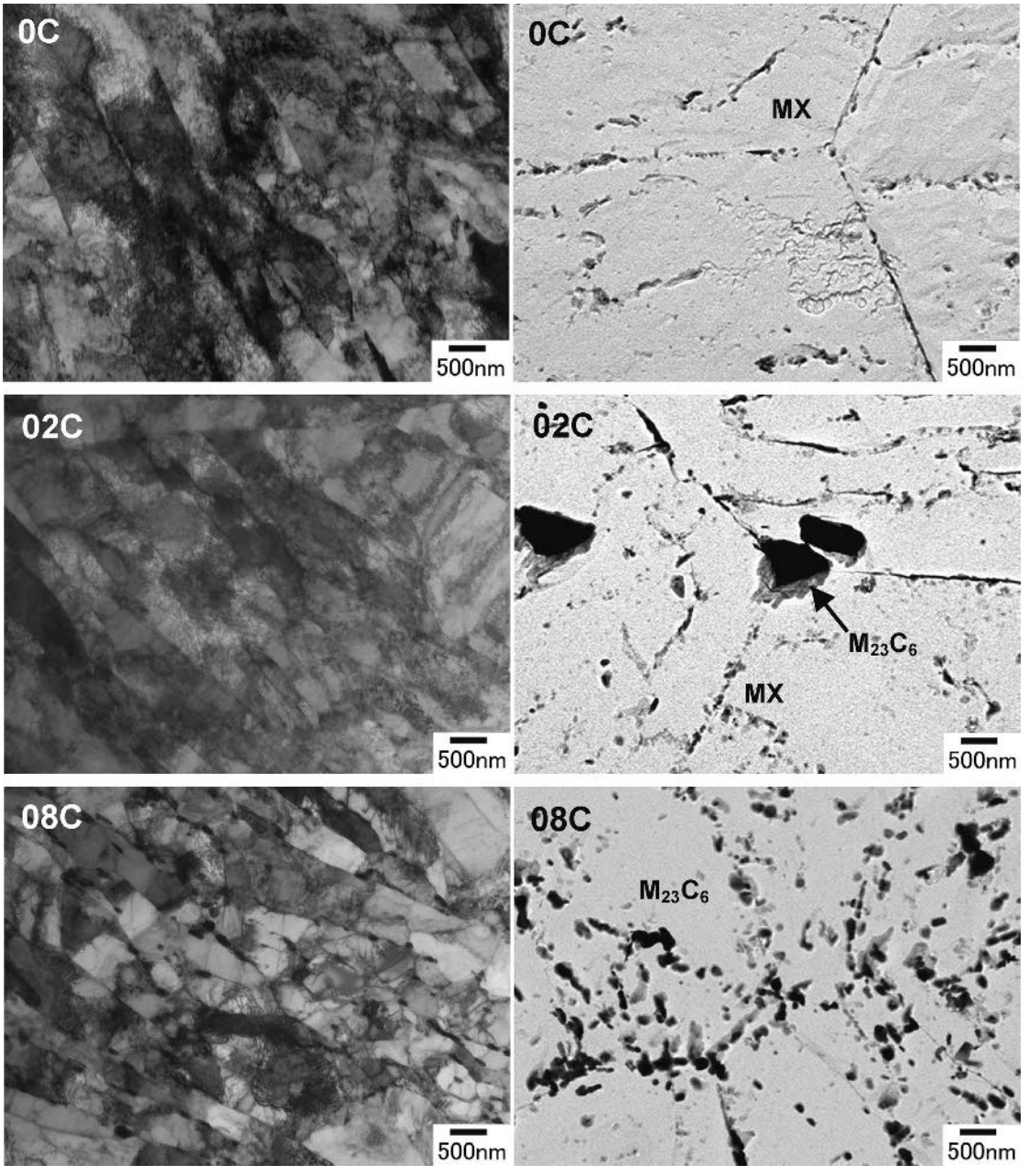


Fig. 7—TEM micrographs of thin films and carbon extraction replicas of 0C, 02C, and 08C steels after tempering.

both dislocation densities and lath widths between 0C and 08C steels is small, especially after tempering, and hence it is suggested that the martensitic structure is similar in the steels.

### B. *Distribution of $M_{23}C_6$ Carbides and MX Carbonitrides after Tempering*

Figure 7 shows the TEM micrographs of thin films and carbon extraction replicas of 0C, 02C, and 08C steels after tempering. Many particles precipitate in the steels. We carried out the observation of replica by the TEM about the steels after normalizing, but no precipitate except inconsiderable impurities was present in the steels. Accordingly, almost all particles in Figure 7 precipitate during tempering. Morphology of precipitates differs greatly among the steels depending on carbon concentration. The size of precipitates in 0C steel is much smaller than that in 08C steel. By EDX analysis, large particles and fine particles are determined as $M_{23}C_6$ and MX, respectively. In 02C steel, large $M_{23}C_6$ precipitate, but the number density of $M_{23}C_6$ is considerably lower than with 08C steel.

Figure 8 gives high-magnification micrographs showing the fine distribution of precipitates in the matrix and along boundaries by observation of replicas for 0C and 08C steels. Very fine MX particles precipitate in the matrix of both steels. In 08C steel, MX with vanadium wings,[10] which consist of niobium carbonitrides in the core and vanadium

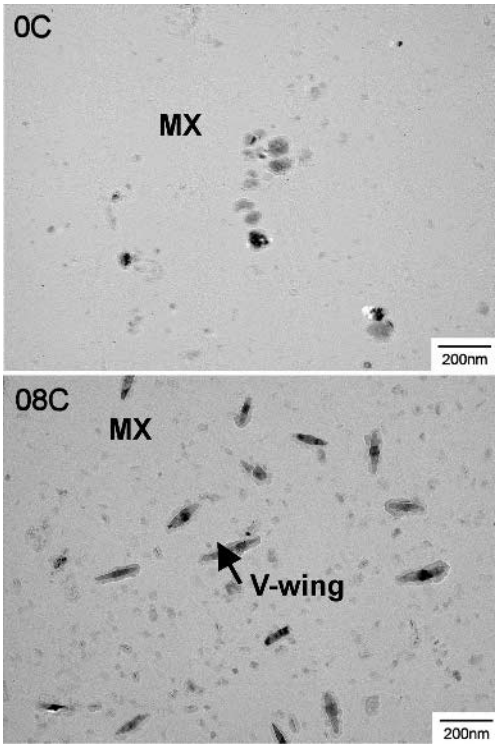


(*a*)

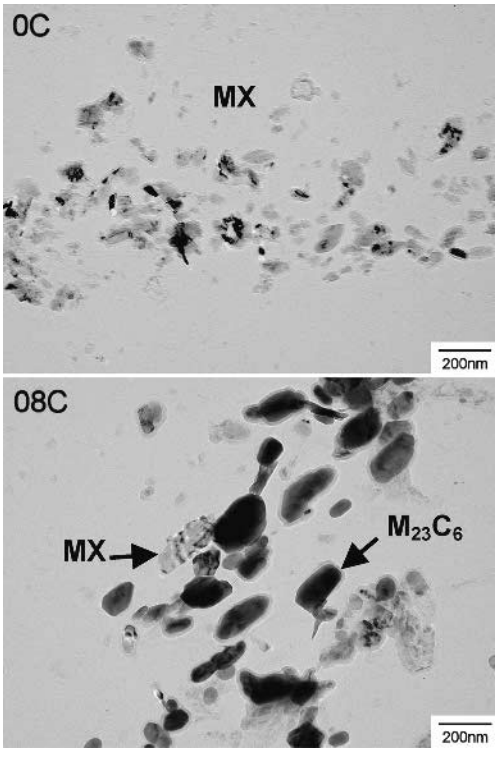


(*b*)

Fig. 8—Precipitated particles inside lath and along boundaries of 0C steel and 08C steel: (*a*) inside lath and (*b*) along boundaries.

carbonitrides on both sides, precipitate here and there, but there is no MX with V wing in 0C steel. From the micrographs, the approximate spacing between MX particles in the matrix in 0C and 08C steels can be estimated to be about 230 and 120 nm, respectively. The sizes of MX particles in the matrix are about 10 nm in both steels. Unlike in the matrix, the distributions of precipitates along boundaries are quite different between the steels. The precipitates along boundaries are almost completely $M_{23}C_6$ in 08C steel. The MX particles precipitate at intermediate positions in $M_{23}C_6$ along boundaries in 08C steel. In contrast, only fine MX particles precipitate densely along boundaries in 0C steel. The size of $M_{23}C_6$ along boudaries in 08C steel is about 200 nm, and the size of MX along boundaries in 0C steel is about 30 nm. Since many fine particles precipitate along boundaries in 0C steel, the effect of strengthening boundaries in 0C steel is larger than that in 08C steel.

In order to investigate the morphology of MX along boundaries in 0C steel in detail, MX precipitating along boundaries were observed using thin films in the TEM. The results are shown in Figure 9. The boundary is confirmed to be a prior austenite grain boundary from observation at lower magnification. Very fine MX, whose sizes are below 10 nm, precipitate densely along the boundary. The EDX analysis shows that the MX contain both vanadium and niobium. The spacing between (111) planes of the precipitate measured from the photograph of the diffraction pattern is about 2.398 Å. The value largely corresponds with that of vanadium nitride, 2.390 Å. From Figure 9, the (100) plane of MX is parallel to the (100) plane of an adjacent ferrite matrix. In the case of MX precipitate in a ferrite matrix, a coherent relationship between MX and the ferrite phase, of the Baker–Nutting type, is indicated.[12] The relationship is as follows:

$$(100)\text{MX}//(100)\text{ferrite},\ [010]\text{MX}//[011]\text{ferrite},\ [001]\text{MX}//[011]\text{ferrite}$$

Consequently, the MX shown in Figure 9 probably have a Baker–Nutting relationship.

Figure 10 shows the mass fraction of vanadium, niobium, and chromium in MX in the matrix and along the boundaries of 0C and 08C steels by EDX with the TEM for replica films. The average values of about 50 MX particles in each test piece are shown in this figure. Light elements such as carbon and nitrogen cannot be analyzed because of inaccuracy of EDX analysis. The results are similar between 0C and 08C steels, but the mass fraction of constituents of MX is different between those in the matrix and along boundaries. The MX along boundaries contain more vanadium and less niobium than those in the matrix.

Figure 11 shows the amount of elements in precipitates in the steels after tempering. The amount of precipitated iron, chromium, and tungsten increases rapidly with increasing carbon content. This indicates that the amount of $M_{23}C_6$ carbides increases with increasing carbon content since these elements constitute $M_{23}C_6$ carbides. Amounts of precipitated niobium and vanadium, which constitute MX, are almost the same among the steels. The amount of MX is not so influenced by carbon concentration and hence the precipitated MX particles are mostly regarded as nitrides, as shown in the results of calculation by Thermo-Calc in Figure 2.

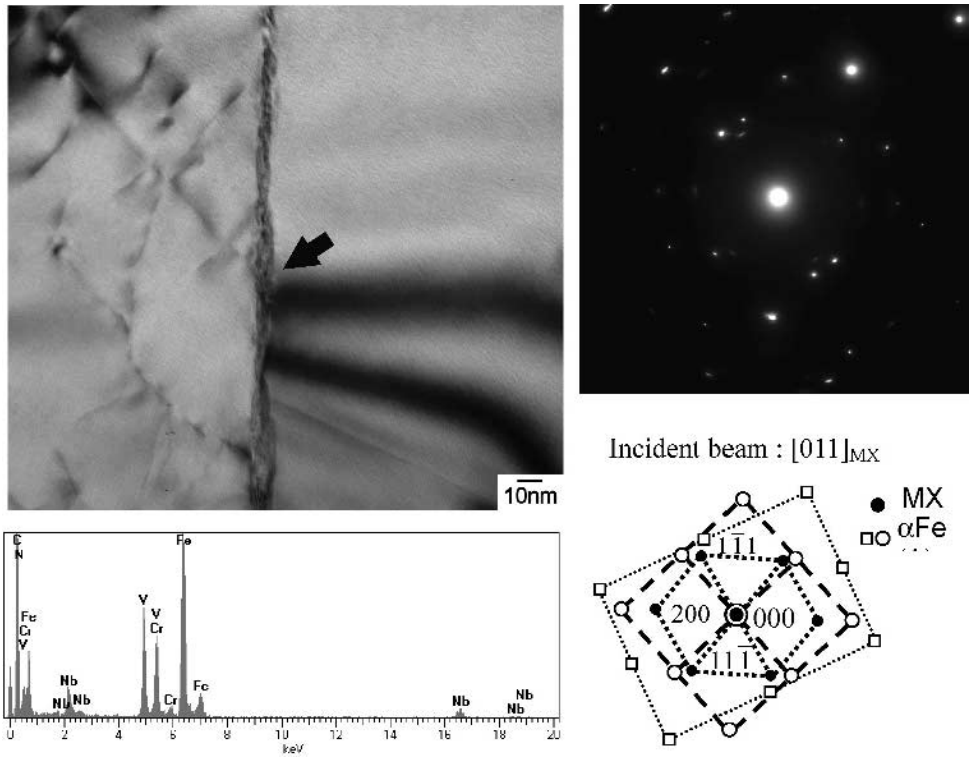


Fig. 9—MX precipitated along boundaries in 0C steel after tempering.

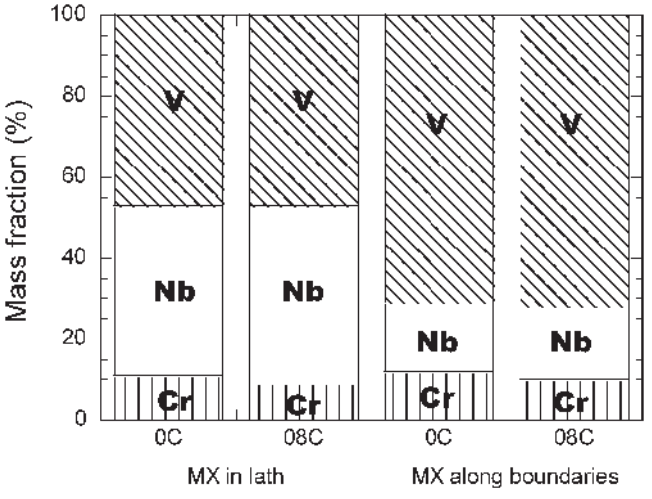


Fig. 10—Fraction of elements in MX measured from replica films by EDX with TEM.

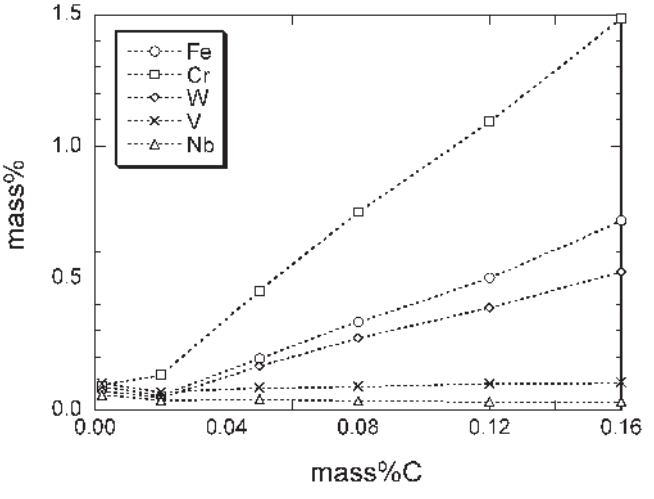


Fig. 11—Amount of elements contained in precipitates after tempering.

## V. DISCUSSION

As shown in Figure 1, the amount of $M_{23}C_6$ increases with increasing carbon content in the results of the calculation by Thermo-Calc. The increase of $M_{23}C_6$ in the calculation corresponds to the increase of iron, chromium, and tungsten estimated experimentally, as shown in Figure 11. The amount of $M_{23}C_6$ increases linearly, but distribution of $M_{23}C_6$ does not change continuously with carbon content. The distributions of precipitates in the steels are categorized into three types depending on carbon content. A schematic diagram of the distribution of precipitates is shown in Figure 12. Regarding 0C steel, no $M_{23}C_6$ precipitates, while fine MX do precipitate. Regarding the steels containing carbon above 0.05 pct, many $M_{23}C_6$ precipitate and the main precipitate along boundaries is $M_{23}C_6$. Regarding 02C steel, the size of $M_{23}C_6$ is quite large and the number density of $M_{23}C_6$ is low. In 02C steel, the degree of supersaturation of elements constituting $M_{23}C_6$ after normalizing is smaller than that in the steels containing more carbon, and hence, the driving force of precipitation of $M_{23}C_6$ in tempering is small and the radius of the critical nucleus grows. Accordingly, the size of $M_{23}C_6$

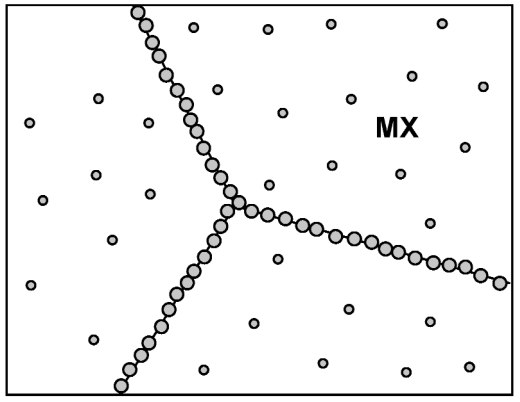


(*a*)

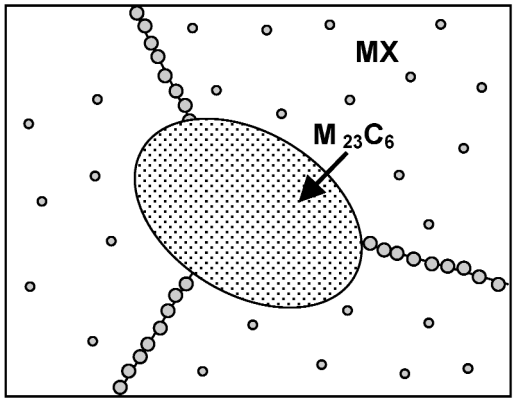


(*b*)

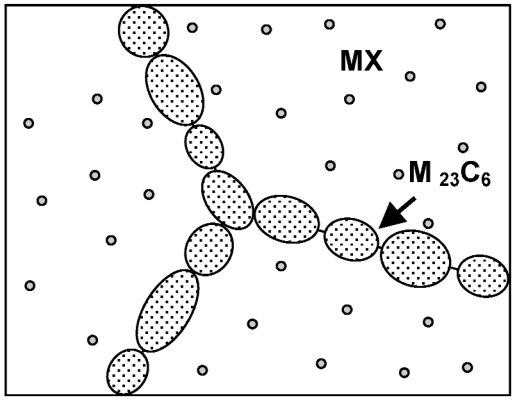


(*c*)

Fig. 12—Schematic diagram of the distribution of precipitates: (*a*) 0C steel, (*b*) 02C steel, and (*c*) 05C to 16C steel.

is quite large and the distribution of $M_{23}C_6$ is sparse in 02C steel. $M_{23}C_6$ precipitate, but the main precipitates along boundaries is MX in 02C steel, as with 0C steel.

In the steels after tempering, MX precipitated both in the matrix and along boundaries. As shown in Figure 10, the mass fractions of constituent of MX in the matrix and that of MX along boundaries are a little different. The MX along boundaries contain more vanadium than those in the matrix. This is probably because the precipitation of vanadium, which is slower than that of niobium,[13] along boundaries is easier and faster than in the case of precipitation in the matrix, because disarrangement of the lattice is large and the driving force needed to precipitate on boundaries is smaller.

Between 0C and 08C steels, the morphology of MX in the matrix is a little different. In 08C steel, MX with V wing sometimes precipitate. In contrast, no MX with V wing precipitate in 0C steel. In the case in which MX with V wing precipitate in the matrix, niobium carbonitride precipitate first as core and vanadium carbonitrides precipitate continuously on the core.[11] It is suggested that many MX particles, containing more vanadium, precipitate along boundaries in 0C steel, and hence, there is not enough vanadium to precipitate as V wing on MX in the matrix.

In order to increase the effect of precipitation strengthening, it is necessary to reduce spacing between particles since the effect is in inverse proportion to the spacing between particles. From the photographs shown in Figure 7, the approximate spacing between particles along boundaries in 0C and 08C steels can be seen to be about 10 and 100 nm, respectively. In some parts of the 0C steel, there is no spacing between MX particles along boundaries since they are connected, as shown in Figure 9. Thus, since many fine MX precipitate densely in 0C steel, it is suggested that the effect of strengthening of boundaries by precipitates in 0C steel is much larger than that in 08C steels. Furthermore, MX do not grow more easily than $M_{23}C_6$ at high temperatures, and hence, it is expected that the small spacing between MX particles in 0C steel is maintained during long-time creep deformation.

## VI. CONCLUSIONS

The change of distribution of precipitates and microstructure with decreasing carbon concentration regarding six kinds of steel containing from 0.002 to 0.16 mass pct C, based on 9Cr-3W-3Co-0.05N-0.007B at 1073 K, was investigated. The following conclusions have been drawn from the present investigation.

1. Fine MX nitrides precipitate densely along boundaries in the steels containing carbon below 0.02 pct, while almost no $M_{23}C_6$ carbides precipitate. It is considered that the effect of precipitation strengthening by MX along boundaries is large since the spacing between MX particles is very small.
2. The amount of precipitation of MX is not influenced so much by carbon concentration, and hence, the precipitated MX particles are regarded mostly as nitrides.
3. The MX with V wing stops precipitating in 0C steel. It is suggested that many MX particles containing more vanadium precipitate along boundaries in 0C steel, and hence, there is not enough vanadium to precipitate as V wing on MX in the matrix.

## REFERENCES

1. E. Cerri, E. Evangelista, S. Spigarelli, and P. Bianchi: *Mater. Sci. Eng.*, 1998, vol. A245, p. 258.
2. F. Abe: *4th Int. Conf. on Recrystallization and Related Phenomena*, The Japan Institute of Metals, Sendai, 1999, p. 289.
3. T. Horiuchi, M. Igarashi, and F. Abe: *Iron Steel Inst. Jpn. Int.*, 2002, vol. 42, Suppl., p. S67.

4. P.J. Ennis, A. Zielinska-Lipec, O. Wachter, and A. Czyrska-Filemonowicz: *Acta Mater*., 1997, vol. 12, p. 4901.
5. E. Orowan: *Discussion in Symp. on Internal Stresses in Metals and Alloys*, Institute of Metals, London, 1948, p. 451.
6. F. Abe, M. Igarashi, S. Wanikawa, M, Tabuchi, T. Itagaki, K. Kimura, and K. Yamaguchi: *Proc. PARSONS, 2000 Advanced Materials for 21st Century Turbines and Power Plant*, The Institute of Materials, London, 2000, pp. 129-42.
7. M. Taneike, F. Abe, and K. Sawada: *Nature*, 2003, vol. 424, pp. 294-296.
8. Lars Hoglund: *Foundation of Computational Thermodynamics*, Royal Institute of Technology, Stockholm, 1997, p. 1.
9. J.A. Bailey and P.B. Hirsch: *Phil. Mag*., 1960, vol. 5, p. 485.
10. T. Maki and I. Tamura: *Tetsu-to-Hagané*, 1981, vol. 67, p. 852.
11. K. Tokuno, K. Hamada, R. Uemori, T. Takeda, and K. Itoh: *Scripta Metal*. 1991, vol. 25, p. 871.
12. R.G. Baker and J. Nutting: *ISI Special Rep*. 1959, vol. 64, p. 1.
13. A. Iseda, H. Teranishi, and F. Masuyama: *Tetsu-to-Hagané*, 1990, vol. 76, p. 36.